PAPER

Properties of the density of shear transformations in driven amorphous solids

View the article online for updates and enhancements.

Properties of the density of shear transformations in driven amorphous solids

Ezequiel E Ferrero[1],[*] and **Eduardo A Jagla**[2]

[1] Instituto de Nanociencia y Nanotecnología, CNEA–CONICET, Centro Atómico Bariloche, (R8402AGP) San Carlos de Bariloche, Río Negro, Argentina
[2] Centro Atómico Bariloche, Instituto Balseiro, Comisión Nacional de Energía Atómica, CNEA, CONICET, UNCUYO, Av E Bustillo 9500 R8402AGP S C de Bariloche, Río Negro, Argentina

E-mail: ferrero@cab.cnea.gov.ar

Abstract
The strain load $\Delta\gamma$ that triggers consecutive avalanches is a key observable in the slow deformation of amorphous solids. Its temporally averaged value $\langle \Delta\gamma \rangle$ displays a non-trivial system-size dependence that constitutes one of the distinguishing features of the yielding transition. Details of this dependence are not yet fully understood. We address this problem by means of theoretical analysis and simulations of elastoplastic models for amorphous solids. An accurate determination of the size dependence of $\langle \Delta\gamma \rangle$ leads to a precise evaluation of the steady-state distribution of local distances to instability x. We find that the usually assumed form $P(x) \sim x^\theta$ (with θ being the so-called pseudo-gap exponent) is not accurate at low x and that in general $P(x)$ tends to a system-size-dependent *finite* limit as $x \to 0$. We work out the consequences of this finite-size dependence standing on exact results for random-walks and disclosing an alternative interpretation of the mechanical noise felt by a reference site. We test our predictions in two- and three-dimensional elastoplastic models, showing the crucial influence of the saturation of $P(x)$ at small x on the size dependence of $\langle \Delta\gamma \rangle$ and related scalings.

Keywords: amorphous solids, yielding transition, density of shear transformations, avalanches, elastoplastic models

(Some figures may appear in colour only in the online journal)

Punctuated dynamics is inherent to many out of equilibrium driven systems. When energy is loaded at a small and fixed rate, the nature of the system is such that this energy is dissipated in sudden bursts of activity typically called slip events or avalanches. This kind of systems are referred to as displaying a stick-slip dynamics. Examples include the relative motion of tectonic plates giving rise to earthquakes [1], the sliding of charge density waves [2], the driven movement of a magnetic interface in thin magnetic films [3], the intermittent motion of rain droplets on a windshield [4] and the plastic rearrangements occurring in amorphous solids under a slow and sustained strain increase [5]. In all these cases, a stationary situation is established in which, on average, the stress (or energy) increase during quiescence periods is equal to the stress (or energy) drop released during avalanches.

Suppose that we drive a system with stick-slip dynamics on its steady state, and we are interested in the statistics of strain increases needed to produce a new slip event, for systems of different sizes. If the system consists on N 'blocks' that can be locally destabilized, one expects that the load needed to trigger the weakest block scales with $1/N$. This is, if we double the system size, the closest instability will be halfway apart in terms of strain increase needed. Equivalently, if we drive the system at a small finite rate, the pace at which we observe slip events doubles when we double the system size. More rigorously, if avalanches have a maximum extent that does not diverge as the system size goes to infinity, then the system is extensive. The previously mentioned balance between accu-

[*] Author to whom any correspondence should be addressed.

mulation and release of energy then implies that if the system size is doubled, the average load increase that has to be applied to generate a new avalanche is halved. While this is the case for most stick-slip phenomena (e.g., friction, depinning, wetting, etc), the behavior of amorphous solids under deformation disobeys this logic. In the deformation of amorphous materials, if we double the system size, the rate at which we observe slip events does not double. It increases, but less; it is *sub-extensive* in the system size. In other words, to trigger the next slip one needs to load *more than expected*. As a consequence, when the system finally yields, the slip of a single block is not enough to compensate the load excess and system spanning avalanches of plastic events emerge. Therefore, the plastic activity is rarely confined to localized plastic events and, instead, it is mostly originated in large structures [6]. This points clearly to the non-extensiveness of the problem. In fact, if we consider conversely that the dynamics of the problem produces system size spanning avalanches, then a doubling in the system size would not duplicate the number of avalanches.

It is now well established that the statistics of the mean strain load $\langle \Delta \gamma \rangle$ needed to trigger consecutive avalanches in the steady state of quasistatically driven amorphous solids has profound consequences on the criticality of the yielding transition [7–9]. In particular, its finite-size scaling is expected to be a manifestation of the distribution of putative shear transformation zones $P(x)$ ($x \equiv \Sigma_{th} - \Sigma$ stands for the local 'stress distance' to the local yielding threshold Σ_{th}) and bounds through scaling relations the possible exponents governing the avalanche size distribution [5, 10–14]. While consensus on this scaling being sub-extensive prevails, i.e., $\langle \Delta \gamma \rangle \sim N^{-\alpha}$, with $0 < \alpha < 1$, there have been conflicting views on the value of α and its justification. On one hand molecular dynamics (MD) simulations [7–9] of model glasses under quasistatic deformation support an universal value of $\alpha \simeq 2/3$, valid both in $d = 2$ and $d = 3$ dimensions. On the other hand, elastoplastic (EP) models for amorphous solids [10, 11] display dimension-dependent values of α.

Despite large advances in the field, theoretical arguments have not taken yet in full account the statistical significance of the $\langle \Delta \gamma \rangle$ sub-extensivity in the steady state. Such a scaling has been well accounted as a justification for system-spanning avalanches of plastic activity in the system; but the fact that it also implies an inherent discrete evolution for the 'local distances to threshold' x was disregarded. In this work, we address this issue, presenting an alternative and consistent picture for the finite-size scaling of $x_{min} \equiv \min_i x_i$. Standing on the ground provided by previous works [15–18], we interpret the evolution of the stress (and thus also x_i) in a generic region of the system as an effective stochastically-driven random walk. Working out the finite-size scaling of the relevant discrete jump in this walk we derive a generic scaling law $\langle x_{min} \rangle \sim N^{-\alpha}$ with $\alpha = 2/3$. In doing so, we revisit the significance and shape of the distribution $P(x)$, which shows a finite limit $P_0 = \lim_{x \to 0} P(x)$ that scales as $P_0 \sim N^{1-\alpha}$ in the thermodynamic limit. This scaling occurs independently of the

eventual value of θ observed at intermediate values of x where $P(x) \sim x^\theta$ can be fitted.

In section 1 we refresh the subject under discussion in a mini-review. In section 2 we motivate and perform an analysis in terms of simple random-walkers problems with exact solutions to understand the effect of discrete steps. In section 3 we rationalize the collective effect of plastic events during avalanches as an effective mechanical noise with a discrete step effect on the 'walks' of local stresses. In section 4 we test our hypothesis in extensive simulations of 2D and 3D elastoplastic models, presenting rigorous finite size analysis for $\langle x_{min} \rangle$ and $P(x)$ in different cases. Finally, in section 5 we summarize our results, that we believe allow to construct a consistent scenario for what seemed *a priori* contrasting results in literature.

1. Overview of the subject

Let us start by briefly reviewing the main concepts and literature results on this topic. In essence, one can think of a yielding material as a fully-connected set of elastoplastic blocks characterized by a local stress Σ_i or, equivalently, a local *distance* to the stress threshold $x_i = \Sigma_{thi} - \Sigma_i$. These blocks evolve according to a global load that drives the x_i values towards zero. When a particular x_j reaches zero, the block yields, reaching a new equilibrium position (at some new, positive value of x_j) while at the same time producing (via elastic interactions) a modification of the values of other x_i all across the system. We say that these are 'mechanical kicks' given to the blocks each time one of the blocks yields. The yielding of block j may produce (due to the mechanical kicks) the yielding of other blocks in cascade. This is the origin of avalanches in the system that characterize the dynamics. Because of this avalanche-dominated dynamics, the stress–strain evolution in the system has a qualitative form as depicted in figure 1. Once in its steady state, a driven amorphous solid performs an interspersed sequence of load periods and slip events when the relevant stress component is monitored. A stationary average value is expected for the stress on a steady state. On top of this average value, stress fluctuations contain information on the physics of the problem. In particular, the average strain increase of the loading periods (referred to as $\langle \Delta \gamma \rangle$) and the average stress-drop during the slip events ($\langle \Delta \Sigma \rangle$) must be proportional in a stationary situation (see figure 1), namely

$$\langle \Delta \Sigma \rangle = B \langle \Delta \gamma \rangle \tag{1}$$

with B an elastic constant.

In a quasistatic athermal dynamics, the stress increment that needs to be applied to trigger a new avalanche is nothing but the minimum x_i across the system, namely x_{min}. Then,

$$\langle x_{min} \rangle = \langle \Delta \Sigma \rangle. \tag{2}$$

Further, energy drops, quantifying the energy dissipated during plastic avalanches, can be easily related to the stress-drops as $\langle \Delta U \rangle = \Sigma_Y \langle \Delta \gamma \rangle V = \frac{\Sigma_Y}{B} \langle \Delta \Sigma \rangle V$; where $V = L^d = N$ is the system volume and Σ_Y is the global yield stress [7, 8]. In fact, the starting point of the current discussion can be traced
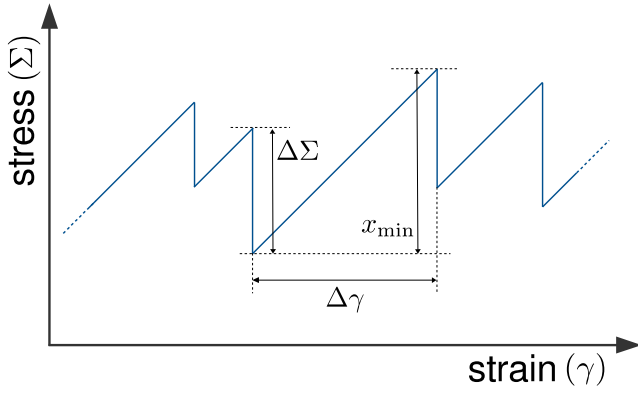
Figure 1. Steady-state stress–strain scheme in the quasistatic shear deformation of an amorphous solid.

back to a series of MD quasistatic simulations [7–9] where the following system-size scaling laws were verified

$$\langle \Delta U \rangle \sim N^{\delta} \quad ; \quad \langle \Delta \Sigma \rangle \sim N^{-\alpha} \qquad (3)$$

holding $\delta + \alpha = 1$, with $\delta \simeq 1/3$ and $\alpha \simeq 2/3$, both in two and three spatial dimensions. Also [19] independently showed compatible results. In reference [8], when thinking on the distribution of possible plastic events, an ansatz was introduced. Arguing that the distribution of energy barriers felt in a quasistatic loading protocol should grow as a power-law, it was proposed for the distribution of local distances to instabilities (x is the generic value of all x_i across the system) the expression

$$P(x) \sim x^{\theta}, \qquad (4)$$

for small x and with $\theta > 0$. Then the distribution of $x_{\min}$ follows a Weibull distribution

$$P(x_{\min}) \sim x_{\min}{}^{\theta} \exp\left(-N x_{\min}{}^{\theta+1}\right), \qquad (5)$$

with its mean value scaling as

$$\langle x_{\min} \rangle \sim N^{-1/(1+\theta)}, \qquad (6)$$

which provides a justification for the scaling of equation (3), linking α and θ:

$$\alpha = \frac{1}{1+\theta}. \qquad (7)$$

Yet, notice that equation (6) does not imply $P(x) \sim x^{\theta}$. The small argument power-law form of the Weibull distribution for $P(x_{\min})$ was verified in the statistics of the 'as-quenched' state or *isotropic* solid state, both in $d = 2$ and $d = 3$ dimensions [7–9]. And it is in fact for this case that the ansatz (4) was proposed [8]. Nevertheless, these pioneer MD simulations could not easily access the whole distribution $P(x)$, and results where only presented for $P(x_{\min})$ [or $P(\Delta\gamma)$].

Luckily, soon after, the problem was addressed by EP model simulations measuring the full $P(x)$ distribution [10]. In there, a plausible law $P(x) \sim x^{\theta}$ was found not only in the 'as-quenched' state but also at the critical stress. The $P(x) \sim x^{\theta}$ ansatz was subsequently extended to describe also the critical steady state in EP simulations [11]; and furthermore,

also the transient regime [20] where a statistics of extended avalanches was equally observed. It was concluded that θ, and therefore α according to the construction, should be dimension and system parameter dependent, which was formalized in an analytic mean-field approach [21]. This theory has the virtue of formally catching a strain-dependence of θ, a feature that is observed in the transient regime both in EP [20, 21] and MD [22–25] simulations. In such transient, the values of θ observed are highly non-universal, depending on system preparation, system parameters and dimension [21, 23, 26].

In the construction summarized in [21], α is expected to follow the same trend as θ all the way from the 'as-quenched' state to the steady-state, keeping the relation $\alpha = 1/(1+\theta)$, and binding α to be also highly non-universal. Nevertheless, one naturally expects θ and α to stop depending on strain in the steady-state, and indeed the literature has collected from the beginning evidence for such expectation [8, 10, 11]. Moreover, we have recently showed that in that limit those exponents are model-independent [15] for a large set of EP model rules; they do depend on dimension though. So, at some point the variation of α and θ with strain should vanish. How that happens, may be a matter of theoretical discussion itself. For the time being, we will focus on the limit of large strains where a self-consistent and stationary stick-slip phenomenon is expected to occur.

Interestingly, in contrast with the case of 'as-quenched' systems, the relation $\alpha = 1/(1+\theta)$ does not seem to hold so well in the numerical results of the steady-state in EP models. For example, in [11] θ is reported to be ~ 0.57 and ~ 0.35 respectively in $d = 2$ and $d = 3$, while α results form the $x_{\min}$ scaling in ~ 0.67 and ~ 0.79 for those cases [27]. More recent EP simulations [28] show $\alpha \simeq 0.675$ combined with $\theta \simeq 2/3$ in $d = 2$. And in [15] we have observed $\alpha \simeq 2/3$ and $\theta \simeq 0.75$ for six different $d = 2$ EP models, pushing the relation $\alpha = 1/(1+\theta)$ even further away from validity. The apparent violation of such relation in the steady state is accompanied by two related observations. First, it is well known from the beginning of this discussions that $P(x_{\min}) \sim (x_{\min})^{\theta}$ does not show up in the steady-state [8, 10]; in fact that law, valid for the 'as-quenched' state, is rapidly suppressed as soon as the applied stress is finite [22, 23]. Secondly, recent numerical results in both MD simulations [25] and EP models [15, 28] have consistently made evident that in the steady state $P(x)$ displays a plateau at small values of x (a non-zero base value, unmistakable in a double logarithmic plot $P(x)$ vs x), and suggested that the finite-size scaling of $\langle x_{\min} \rangle$ can be dominated by the behavior with system size of the finite asymptotic value of $P(x)$ at vanishing x rather than by the exponent θ.

What seems to be clear, at least, is that the plain assumption $P(x) \sim x^{\theta}$, which was somehow inherited from the 'as-quenched' phenomenology and carried by for all values of strain, is insufficient in the steady state. Nevertheless, for instance, a scaling relation based on equation (7), and linking the exponents τ, d_{f} that describe the distribution of avalanche sizes with the exponent θ (namely, $\tau = 2 - \frac{\theta}{1+\theta}\frac{d}{d_{\mathrm{f}}}$) has been largely adopted in the EP models literature [5, 12, 14, 29], always accepted without further justification and relying sometimes on generous error bars for the exponents. Something is

missing in the understanding of what controls α, which might cause that even the latter relation among exponents should be revised. In this work we address the issue, admittedly limiting ourselves to the steady-state case, were we expect universal values of α [8, 15, 22].

1.1. A mean-field approach to yielding

In [21], Lin and Wyart extending a work by Lemaitre and Caroli [30] presented a mean-field approach which is based in the assumption that the mechanical kicks produced by yielding sites on every other site can be taken from a given distribution defined once and for all, independently of the state of the system, and, more importantly, that this distribution is heavy-tailed. Based in the instantaneous values of the local 'stress-distances' to threshold $x_i = \Sigma_{\text{th}i} - \Sigma_i$, the mean-field dynamics can be described as follows. If at time t the block j yields (reaches $x_j \leqslant 0$), it is re-injected at a positive value of x_j (e.g. $x_j = 1$) and the rest of the blocks suffer mechanical kicks ξ_i taken form a distribution $w(\xi_i)$ (see equation (9)) with zero mean $\langle \xi_i \rangle = 0$,

$$
\begin{aligned}
x_j(t+1) &= 1, \\
x_i(t+1) &= x_i(t) + \xi_i - \frac{1 - x_j(t)}{N-1},
\end{aligned}
\tag{8}
$$

where the last term grants stress conservation and in this case the re-injection point has been chosen to be $x = 1$.

A highly distinctive feature of yielding phenomena lays in the fact that the mechanical noise distribution $w(\xi_i)$ comprises both positive and negative values. This feature has its roots in the Eshelby response observed upon plastic events in amorphous materials and described in appendix A. Once this is guaranteed, these mean-field models behave qualitatively like elastoplastic models of amorphous solids [5]: there is a global yield stress Σ_Y such that for $\Sigma < \Sigma_Y$ the dynamics eventually stops, corresponding to the solid phase. For, $\Sigma > \Sigma_Y$ the dynamics does not stop and is characterized by a global strain rate. The dynamics therefore can be rationalized as 'random walks' of the elastoplastic blocks in the x-coordinate, with an absorbing boundary at $x = 0$ [21], as qualitatively depicted in figure 2. This representation of the yielding phenomenon allows us to start by analyzing simple random-walk processes and extrapolate conclusions from there, see section 2.

The signed nature of the mechanical noise gives rise to a density depletion of $P(x)$ close to the absorbing boundary [11, 15]. In contrast to the case of a purely positive interaction among sites where each destabilized block tends to destabilize the others, the signed kicks allow some blocks to escape the boundary and survive longer without yielding. This is the hand-waving argument for the existence of a pseudo-gap $P(x) \sim x^\theta$ with $\theta > 0$. Formally solving the stochastic problem of equation (8), Lin and Wyart concluded that θ depends continuously on the applied shear stress, non monotonically and without signs of universality at the yield stress. The latter observation leaves little room for the expectation of universal exponents among different EP models, not to talk about MD simulations. We will contrast this view.
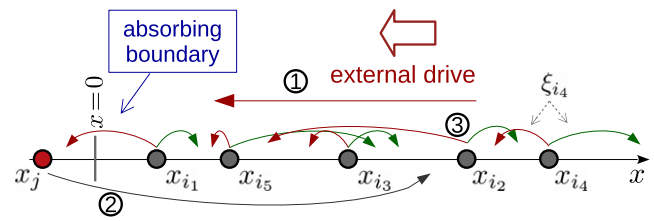

Figure 2. Schematic wandering of the x_i values. The external drive pushes everyone towards zero ①. When x_j yields, it is re-injected ② at a positive value of x and all the remaining x_i receive kicks ξ_i ③. These kicks can be either positive or negative and of different intensities (as illustrated by the arrows' different colors and lengths), according to the prescribed distribution $w(\xi)$. The signed nature of the mechanical noise allows the system to 'forecast' the boundary [11] and creates a density depletion of $P(x)$ close to $x = 0$.

1.2. Alternative views

The mean field construction in [21] is based on the assumption of a mechanical noise $w(\xi)$ of the form

$$
w(\xi) \sim \frac{1}{|\xi|^{\mu+1}}
\tag{9}
$$

in the particular case of $\mu = 1$, that the authors claim is the only value with 'physical meaning' to be expected to occur.

The necessity of the particular value $\mu = 1$ has been recently questioned [15–17]. In particular, it was argued the assumption $\mu = 1$ in equation (9) is not in agreement with the observation of sub-extensive avalanches dominating the plastic activity in the quasistatic limit [15, 16]. Other values of μ with $1 < \mu < 2$ acquire physical meaning after the mechanical noise is properly redefined (see section 3). And, in fact, a value of $\mu \simeq 3/2$ was found to be consistent with the mechanical noise sensed numerically in six different EP models in two dimensions [15]. Recently, the physical case of $1 < \mu < 2$ has been also addressed in [31] both for the aging and steady regimes, finding no reasons to discard it. Interestingly, the mean field theory of [21] yields a well defined value of $\theta = \mu/2$ when $1 < \mu < 2$, independent on other parameters. Yet, a uniquely-defined value of $\theta = \mu/2$ would still fail to explain through equation (7) the value of α observed in both MD and EP simulations. Remarkably, it has been recently observed quite clearly in both EP [15, 28] and MD [25] simulations that the true shape of $P(x)$ at small values of x deviates from a pure power-law $\sim x^\theta$, and has a finite limit

$$
P_0 \equiv \lim_{x \to 0} P(x) \neq 0.
\tag{10}
$$

Namely, for any finite system size, $P(x)$ has a *plateau* [when $P(x)$ is presented in a logarithmic plot] at small enough x. As we will argue in the following, the plateau in $P(x)$ is originated in the discrete nature of the mechanical noise that produces the 'kicks' felt by x_i. These kicks (that we consider to be generated by extended plastic avalanches elsewhere in the system) push each x_i to perform a (non-Gaussian) random walk. In this scenario, it is the system size scaling of P_0 what dominates the scaling of $\langle x_{\min} \rangle$ and controls the values of α and δ in equation (3), which now turn to be compatible with the independent exponent $\theta = \mu/2$.

In the following, we elaborate on this picture. Our work deals largely with providing analytical arguments and numerical support for the system size dependence of P_0 and $\langle x_{\min} \rangle$ and conciliates them with the existence of a well defined value of θ that indeed describes an intermediate region of x values where $P(x) \sim x^\theta$.

2. Simple random walks and the *P(x)* plateau

We analyze first a simple case. Consider a variable x_i performing a random walk in the interval $[0, 1]$, with absorbing boundary conditions. When x_i moves out of the interval, it is 'absorbed' and re-injected in some random way [27]. In the case of a continuous time random walk (a Wiener process), and when the reinjection is done proportionally to the local value of the probability, the form of the distribution of x_i values observed along time in the steady state can be analytically computed to be $P(x) = \frac{\pi}{2} \sin(\pi x)$. For small x it behaves as $P(x) \sim x$, i.e. $\theta = 1$. If we consider N variables ($N \gg 1$) performing the same random walk, the minimum among them will be in the region in which $P(x)$ is linear, and we will have $P(x_{\min}) \sim x_{\min} \exp(-N x_{\min}^2)$, and $\langle x_{\min} \rangle \sim N^{-1/2}$.

The random walks that we introduced in the previous section to describe the phenomenological dynamics of yielding are inherently discrete, and one needs to investigate the consequences of this fact on $P(x)$. In fact, for a *finite step* random walk, although the overall form of $P(x)$ is the same as before, there is a small correction at small x that depends on the step size, and has a strong effect on the value of $x_{\min}$. Let us think for a moment of a particle performing a *discrete* random-walk characterized by a step that is Gaussian-distributed, with a dispersion σ. Assuming the particle is at some position x_0 at a given step, the next jump makes x to be distributed as $P(x) \sim \Theta(x)\Theta(1-x)\exp[-(x-x_0)^2/2\sigma^2]$, where the Heaviside functions Θ appear because of the absorbing boundary conditions. We note that the value of $P(0^+)$ is finite. It turns out that this effect remains in the full solution for the stationary form of $P(x)$. So, the discrete nature of the steps taken by x_i suffices to explain the finite limit of $P(x)$ as $x \to 0$. In figure 3 we see the distribution of $P(x)$ for Gaussian random walks with different magnitudes of the average elementary step, namely, different width σ of the Gaussian 'kicks'. Figure 3(a) shows the stationary distributions in lin–lin scale, figure 3(b) shows them in log–log scale, and the scaling proposed in figure 3(c) shows that the value of P_0 is proportional to σ.

The situation is conceptually identical in the case in which we consider generalized RWs with a non-trivial Hurst exponent H; this is, random walks generated by jumps ξ drawn from a heavy-tails distribution of the form

$$w(\xi) \sim \frac{1}{|\xi|^{\frac{1}{H}+1}}, \tag{11}$$

for large $|\xi|$ with $1/2 < H < 1$. Note first of all that in this case, the 'typical jump' or distribution width σ cannot be defined as being variance of the distribution because of its heavy tails, but it can be alternatively defined as $\sigma \equiv \langle |\xi| \rangle$. As
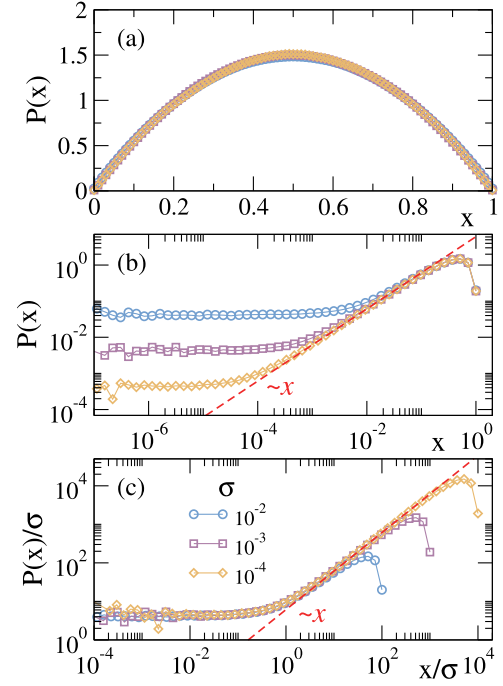

Figure 3. Numerically determined probability distribution for a variable x performing a standard (Gaussian) RW in the interval $(0, 1)$ with absorbing boundary conditions and random reinjection. Different curves correspond to different values of the width of the single step distribution, as indicated. (a) Linear scale. (b) Log scale to emphasize the behavior at low x. The straight line shows the expected asymptotic limit for $\sigma \to 0$. In (c) the axis are rescaled with σ to show that the value $P(0)$ scales as σ.

it was the case for a Gaussian variable, in the limit of vanishingly small jumps (i.e., $\sigma \to 0$) RWs, the form of $P(x)$ for x close to zero is still expected to be $P(x) \sim x^\theta$, where now $\theta = 1/(2H)$ [21]. Yet, for finite σ, a finite value for P_0 appears, as shown in figure 4 for $H = 2/3$. For concreteness, in this numerical example we have taken the distribution $w(\xi)$ to be given by equation (11) if $|\xi| > \xi_0$, and $w(\xi) = 0$ if $|\xi| < \xi_0$. This distribution has a width $\sigma = \langle |\xi| \rangle = \xi_0/(1-H)$. We see that the limiting value of P_0 as a function of σ scales as $P_0 \sim \sigma^{3/4}$ (figure 4(c)). In the generic case with $1/2 < H < 1$, P_0 scales as

$$P_0 \sim \sigma^{1/(2H)} \sim \sigma^\theta. \tag{12}$$

This can be justified by noticing that close to $x = 0$, σ is the only possible scaling quantity with the same dimension as x. Then we can write

$$P(x) = P_0 f(x/\sigma) \tag{13}$$

with $f(u) \simeq 1$ for $u \ll 1$. On the other hand, for $x \gg \sigma$ (but still 'small') we must have $P(x) \simeq Cx^\theta$ with C independent of σ, therefore implying equation (12). In other words, σ marks a scale crossover below which the distribution of x values tends to a constant [32].

Finally, notice that everything we have said for the steady state distribution $P(x)$ populated along time is also true if we populate the distribution with the x_i values of many independent walks in their steady state.
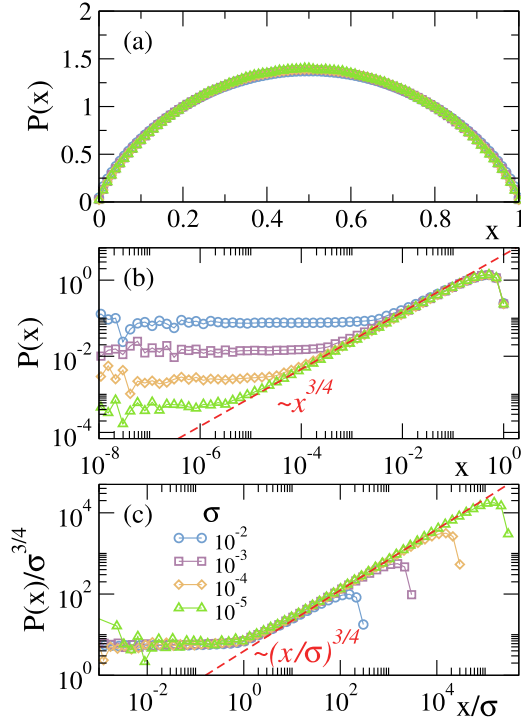
Figure 4. Probability distribution for a variable x performing an RW with Hurst exponent $H = 2/3$ in the interval $(0, 1)$ with absorbing boundary conditions and random re-injection. Different curves correspond to different values of the width of the single step distribution. (a) Linear scale. (b) Log scale to emphasize the behavior at low x. The straight line shows the expected asymptotic limit for $\sigma \to 0$. In (c) the axis are rescaled with σ to show that the value P_0 scales as $\sigma^{-3/4}$ ($\sigma^{-1/2H}$ for a generic H).

2.1. N random walks without or with drift

Let us consider then N independent random walkers subject to the following protocol. Now, starting form a condition where every x_i is in the interval $(0, 2)$ we look for the minimum x_i, that we indicate as $x_{\min}$. Every site is shifted by an amount $-x_{\min}$. The site resulting with $x_i = 0$ is re-injected in the box at $x_i = 1$ and everyone updated by a (randomly) signed random quantity ξ taken from a distribution similar to equation (11) ($\mu = 1/H$)

$$w(\xi) = \frac{A}{M_N} \frac{1}{|\xi|^{\mu+1}}, \qquad (14)$$

but with upper and lower cutoffs set to $\xi_{\mathrm{up}} = (2A/\mu)^{\frac{1}{\mu}}$ and $\xi_{\mathrm{lo}} = (2A/\mu)^{\frac{1}{\mu}} M_N^{-\frac{1}{\mu}}$ for it to be normalized [21]. Importantly, here M_N is an N-dependent parameter, frequently chosen as N itself (see [21]). In the simulations of this toy model we will use $M_N = 1/x_{\min}$ for reasons that will be clearer later on [33]. Every site resulting in $x_i \leqslant 0$ (and eventually in $x_i \geqslant 2$) after the random kicks is also re-injected at $x_i = 1$ (but not producing further kicks). The N walkers feel these kicks independently, yet they are drifted globally by $-x_{\min}$ after each kick update. In order to clearly identify the effect of such global drift, we will also analyze the case where we avoid the global drift step and simply: re-inject the site with the minimum x_i, give random kicks to everyone and further re-inject those that go out of the box.
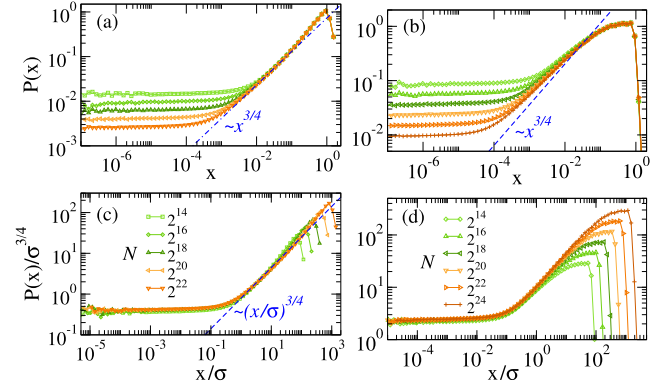

Figure 5. Probability distribution populated by N variables x_i subject to a dynamics of random kicks taken from a heavy tailed distribution like the one in equation (14), with Hurst exponent $H = 2/3$ and $A = 0.1$. Sites absorbed at the boundaries are re-injected in $x = 1$. Different curves correspond to different $\sigma \sim M_N^{-1/\mu} \sim N^{-4/9}$ *left*: without drift: (a) raw-data, (c) rescaled with σ to show $P_0 \sim \sigma^{-1/2H}$. *Right*: with drift. (b) Raw-data, (d) rescaled with σ.

In both protocols, with and without drift, a steady state is established after a transient and the resulting $P(x)$ distributions are shown in figure 5. We can see that the drift couples the dynamics of the walkers and produces the effect of a 'belly' on the curves that delays the decrease of $P(x)$ as we sense x decreasing. The choice of the parameter A now becomes relevant. If A is small, the drift effect overtakes good part of the $P(x)$ distribution and it masks the power-law regime which gets difficult to determine, forcing us to simulate very large systems (or very small σ). If instead A is big enough (closer to 1) the drift effect is much diminished (data not shown). In any case, when a reasonably large power-law region is granted, the θ exponent is preserved for any A, $\theta = \mu/2$ provided that $1 < \mu < 2$. Notice that, despite this 'belly' effect, the existence of a plateau at small x is unchanged, and the predictions $P_0 \sim \sigma^\theta$ still holds, as can be seen in the data collapse of figures 5(b) and (d).

The dynamics that we have just described can be though as a mean-field model for a system of EP blocks with local thresholds where each of them feels an external drive and a noise represented in $w(\xi)$. We will now analyze a spatially extended system of driven interacting blocks in this context.

3. Effective mechanical noise of an interacting system and the *P(x)* distribution

Let us imagine a coarse-grained representation of an amorphous material under deformation, represented by a scalar stress Σ_i on each block and local yielding thresholds $\Sigma_{\mathrm{th}i}$. The variables of interest will be the local distances to threshold $x_i = \Sigma_{\mathrm{th}i} - \Sigma_i$. Our argumentation line is based on the analysis of the mechanical noise felt by a given site of such a system, caused by the plastic activity elsewhere and governing the 'wandering' of x_i.

For the results of the previous section to be applicable to the present case, this noise must consist *ideally* of independent, uncorrelated kicks. As previously mentioned, references

[21, 26] present a mean-field model considering kicks of a mechanical noise generated by single Eshelby events. We will refer to these kicks generated by single sites as 'elementary' kicks. The approximation of reference [21, 26] describes qualitatively well the overall phenomenology observed in numerical simulations, but fails in predicting the exponents observed, at least below $d = 4$. This discrepancy was indeed ascribed to the presence of 'dimensional effects' or correlations between the elementary kicks produced in different positions of the system. We believe that the quantitative predictive power of this kind of analysis can be improved, still keeping the 'mean-field' character of the approach, by noticing and taking into account that elementary kicks are not independent. Elementary kicks produced by sites that participate of the same avalanche are highly correlated among them, but those from different avalanches are not. This fact allows us to build a mean-field approach based on independent non-elementary kicks. One possible choice is to define them as the integrated kicks given by avalanches, that in the quasistatic limit are by definition uncorrelated events.

The fact that the uncorrelated mechanical noise under consideration is produced by *avalanches* as a whole is the reason why now μ in equation (14) can be different from the value $\mu = 1$ that was obtained considering the effect of hypothetical uncorrelated elementary kicks instead [21]. Actually, this alternative approach of avalanche-level noise was already followed in [15, 17]. Simulations of different EP models in two dimensions produce in a test site a noise characterized by a Hurst exponent $H \simeq 2/3$; which from the point of view of the mechanical noise is equivalent to consider that such noise is taken randomly from a distribution like equation (14) with $\mu \simeq 3/2$. With that being proved to be effectively the case for a fully interacting system [15, 17], we cannot expect anything different for its full distribution $P(x)$ than the features discussed in previous sections.

3.1. Finite size scaling of the P(x) plateau

The mechanical noise represented by equation (14) contains as a fundamental parameter the value of μ (or $H \equiv 1/\mu$). A second property of the distribution that has an important physical impact is its 'width' σ. In particular, we are interested in how it scales with system size N. The lower cutoff of the distribution $\xi_{\mathrm{lo}} = (2A/\mu)^{\frac{1}{\mu}} M_N^{-\frac{1}{\mu}}$ is related to the system size and fixed by normalization. If $1 < \mu < 2$, the width σ can be shown to be proportional to ξ_{lo}, and so

$$\sigma \sim M_N^{-1/\mu}. \tag{15}$$

It will be the finite-size behavior of the lower cutoff in $w(\xi)$, the noise produced by the far away plastic activity, what will dominate the scaling of interest. There is also an upper cutoff for the kick distribution, ξ_{up}, but that is related with the strongest, nearest plastic events, and independent on the system size [21, 26].

We have shown in the previous section that any finite step random walk process of a variable x with absorbing boundaries, subject to such a random noise with $1 < \mu < 2$ implies

that in the steady state

$$P(x) \sim x^\theta \quad \text{for } x \gtrsim \sigma \tag{16}$$

$$P(x) \sim \sigma^\theta \quad \text{for } x \to 0. \tag{17}$$

where $\theta = \mu/2$, and σ is the 'width' of the distribution $w(\xi)$, as previously defined. For instance, possible functional forms for $P(x)$ at small x are $P(x) \simeq \sigma^\theta + x^\theta$ or $P(x) \simeq (\sigma + x)^\theta$. Furthermore, we have shown that N random walkers, coupled by a common global drift generate the same limiting form of $P(x)$ as $x \to 0$.

The missing ingredient to make connection with the actual mechanical noise felt by a given block in an amorphous solid is to work out the explicit dependence of M_N in equation (14) on the system size N, and use it to calculate the scaling of σ (equation (15)) and thus the N-dependence of $\langle x_{\min} \rangle$. Note that the approach of [21, 26] uses $M_N = N$ which implicitly considers that each of the N sites produces independent kicks on the generic block i, perturbing x_i. We would like to stress here that this is clearly not realistic. Furthermore, in careful consideration, it goes itself against the basic feature of yielding phenomena displaying size-spanning avalanches and subextensive scaling for the rate of plastic events. Using $M_N = N$ and $\mu = 1$ in equation (14) implies somehow extensivity if kicks are supposed to be independent. Instead, we think on the total noise produced by one avalanche. Among the marginal kicks that a site receives (the ones that it almost fail to catch because of working in a finite system N), the dominant one is not the kick coming from a single site at the maximum possible distance, but the largest possible kick coming from such a distance. That is, a kick coming from the largest avalanche at the largest distance. If equation (14) represents the distribution of kicks generated by individual avalanches in the system, the value of M_N must be chosen in accordance with this interpretation.

The dependence of M_N on system size N can be worked out as follows. Consider two systems with different sizes N_1 and $N_2 > N_1$, and suppose that we want to compare the number of kicks of intensity ξ produced onto some reference site when a fixed (long) deformation strain is applied to the system. The Eshelby interacting kernel decays in space as $\sim 1/r^d$, and this implies that increasing the system size from N_1 to $N_2 > N_1$ does not produce new large kicks [34], but instead increases the number of small ones, those generated at large distances in the system with N_2 sites. This means that if we plot the density number of kicks observed at a given site as a function of the kick magnitude, we would obtain a plot as the one qualitatively depicted in figure 6(a). The portion of these curves following the $1/|\xi|^{\mu+1}$ law will be mostly indistinguishable for the two system sizes. Now, in order to plot the probability distribution $w(\xi)$, as shown in figure 6(b), it is clear that we have to divide by the total number of avalanches (kicks) that occurred in each case. This is why M_N in equation (14) must be considered to be proportional to such a number. In other words, M_N and the average size of avalanches in the system, noted $\overline{S}$, must be related through

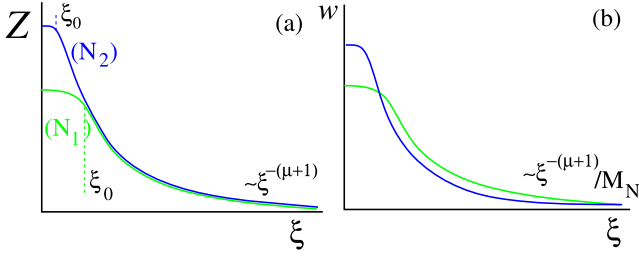$$M_N \sim N\overline{S}^{-1} \sim \langle \Delta\Sigma \rangle^{-1} \tag{18}$$

Figure 6. (a) A schematic plot of the number density of kicks Z of a given intensity ξ observed in systems of two different sizes N_1, and $N_2 > N_1$. The two curves differ below the small size threshold ξ_0 but are coincident in the heavy tail part, for large ξ. (b) The two curves in (a) normalized to become the probability distribution $w(\xi)$. The normalizing factor is the number M_N of avalanches that occur in the two systems under the same increase of external strain.

(which, together with equation (2) justifies our choice for $M_N \simeq 1/x_{\min}$ in the toy model of the previous section 2.1). Now, collecting the results of equations (2), (15) and (18) we arrive at the important result [35]

$$\sigma \sim \langle x_{\min} \rangle^{1/\mu}. \tag{19}$$

Introducing this into equation (17) we get

$$P_0 \sim \sigma^\theta \sim \langle x_{\min} \rangle^{1/2}, \tag{20}$$

since, for $1 < \mu < 2$, $\theta/\mu = 1/2$ [21]. Remarkably, this result is independent of μ in such range.

We are now only one step away from our general scaling results. As mentioned before, recent results in simulations of different EP models [15, 28] and also in MD simulations [25] have shown that (i) a plateau exists for $P(x)$ at vanishing x, but also that (ii) $\langle x_{\min} \rangle$ shifts towards the plateau region of $P(x)$ as the system size N is increased. This can now be analytically justified: from (16) and (17) the crossover between the plateau and the power-law region is expected at $x_{\text{cross}} \simeq \sigma$. Combined with equation (19), this provides $x_{\text{cross}} \sim \langle x_{\min} \rangle^{1/\mu}$. For any $\mu > 1$, this tells that $\langle x_{\min} \rangle$ becomes lower than x_{cross} for large N. In practice, crossovers can be very broad, yet, in the limit $N \to \infty$ the following relation holds

$$\langle x_{\min} \rangle P_0 \simeq 1/N. \tag{21}$$

Using equations (20) and (21) we finally obtain the two important predictions:

$$\langle x_{\min} \rangle \sim N^{-2/3}. \tag{22}$$

and

$$P_0 \sim N^{-1/3}. \tag{23}$$

Notice further that if we assume $P(x) \simeq P_0 + x^\theta$, using equation (20): $P(\langle x_{\min} \rangle) \simeq \langle x_{\min} \rangle^{1/2} + \langle x_{\min} \rangle^\theta$. And, provided $\theta = \mu/2 > 1/2$, the second term becomes negligible over the first when $\langle x_{\min} \rangle$ is small enough. We then could also expect a good ansatz to be:

$$P(\langle x_{\min} \rangle) \simeq \langle x_{\min} \rangle^{1/2}. \tag{24}$$

Followed up from equation (20), the latter would interchange P_0 by $P(\langle x_{\min} \rangle)$ in every subsequent expression. In the limit

$N \to \infty$ both formulations are equivalent, since we expect $P(\langle x_{\min} \rangle)$ to be part of the plateau and identical to P_0. Notice nevertheless that equation (24) (and the ones derived from it) may work well even before reaching that limit.

The scalings provided by equations (22) and (23) (or alternatively $P(\langle x_{\min} \rangle) \sim N^{-1/3}$) is quite generic, as it does not depend on the actual value of μ neither on the dimension of the problem. Even more, it is highly stimulating, since it agrees with the original observations of the $\langle x_{\min} \rangle$ scaling in MD simulations [7, 8] both in $d = 2$ and $d = 3$. Yet, there are assumptions implicitly made in their deduction that can limit their validity. For instance, our construction does not account for anisotropy effects on the dimensions composing the system, which could affect the scaling of any observable with the global system size N. Such an effect appears clearly when considering three dimensional systems, as we discuss below. In addition, equations (22) and (23) do not apply in the case of a model with a (quenched) random kernel, that we describe in appendix B, mainly due to the failure of the argument about the scaling of σ with N. In the next section we test the predictions of equations (22) and (23) in EP models in dimensions $d = 2$ and $d = 3$.

4. Elasto-plastic models in 2 and 3 dimensions

We now present results of quasistatic simulations of spatially extended EP models. We will limit ourselves in particular to the Picard's model [37]. Details about model definition and simulation protocols can be found in the appendix A, and data was produced with essentially the same codes used in [15].

4.1. Two-dimensional systems (2D)

We start with the $d = 2$ case. Figure 7 shows the distribution $P(x)$ for different system sizes $N = L \times L$. We have collected the values of $x \equiv \Sigma_{\text{th}} - \Sigma$ (see appendix A for parameters definitions) from every block in the system for several configurations in the steady state right after an avalanche has finished and before loading the system to the next avalanche. As discussed in previous sections, $P(x)$ displays—also in this fully spatial model—an excess of probability at $x = 0$, evidencing the occurrence of a naturally emerging discrete step for the wandering of the x values. Already from the upper panel (figure 7(a)) it is evident the settling of a system-size dependent plateau at $x \to 0$. This plateau occurs systematically at smaller values of x as L increases. The form of $P(x)$ has more structure than in the random-walk experiments of section 2. Now the crossover region between the power-law regime and the plateau is broader, the power law range is shrunk due to the natural existence of a global drift, and for small systems $P(x)$ even displays an 'S' shape before cutting-off when x becomes order 1. Yet, we can identify for the largest system size a power-law regime spanning two orders of magnitude in x ([$\sim 8.10^{-4}, \sim 8.10^{-2}$]) in excellent agreement with x^θ with $\theta = 0.75$ (the value expected when $\mu = 3/2$ in the discussion of section 3). Let us now check the validity of our predictions in equations (22) and (23). In figure 7(b) the same data of panel
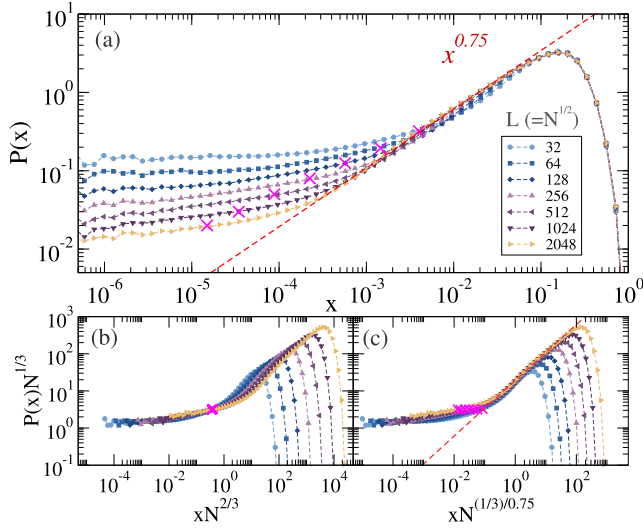
Figure 8. Dependence of $\langle x_{\min}\rangle$, P_0 and $P(\langle x_{\min}\rangle)$ with system size N for 2D Picard's model.

Figure 7. Distribution of local distances to threshold $P(x)$ in the quasistatic driven steady state of Picard's 2D model. (a) The $P(x)$ distributions. Different linear system sizes $L = \sqrt{N}$ are represented with different colors/symbols as declared in the label. Pink crosses indicate the location of $\langle x_{\min}\rangle$ for the different system sizes.
(b) $P(x)N^{1/3}$ vs $xN^{2/3}$ testing the scalings of equations (22) and (23).
(c) $P(x)N^{1/3}$ vs $xN^{(1/3)/0.75}$ to preserve the power-law regime $\sim x^\theta$ with $\theta = 0.75$ observed in the main plot at intermediate values of x.

(a) is plotted as $P(x)N^{1/3}$ vs $xN^{2/3}$. The magenta crosses indicate the position $[x_{\min}, P(x_{\min})]$ on each $P(x)$ curve [36]. The coincidence of the horizontal coordinate of these points is the indication that equation (22) is very well satisfied. According to equation (23) we also expect that the plateaus of all curves in figure 7(b) level up. We see that they do but not perfectly. Instead, note that the values of $P(x)$ at $x = \langle x_{\min}\rangle$ (i.e., the vertical coordinate of the crosses) do become coincident in figure 7(b), fulfilling better the combination of equations (22) and (24)

$$\langle x_{\min}\rangle P(\langle x_{\min}\rangle) \sim 1/N. \tag{25}$$

Figure 7(b) is built to display the combined scaling of $\langle x_{\min}\rangle$ and P_0 [or $P(\langle x_{\min}\rangle)$]. If instead we want to get a collapse of the power-law range of the $P(x)$ distribution for different system sizes, we must preserve the power-law exponent in the transformation. This is done in figure 7(c) where we plot $P(x)N^{1/3}$ vs $xN^{(1/3)/0.75}$, according to the observed $\theta \simeq 0.75$. Following our generalized mean-field picture the value $\theta \simeq 0.75$ observed in the 2D EP model corresponds to a mechanical noise with a Hurst exponent $H = \mu^{-1} \simeq 2/3$ ($\mu = 2\theta \simeq 3/2$). A direct characterization of the mechanical noise to verify this value was already presented in [15, 17], showing a concurrence of different two-dimensional EP models around the Hurst exponent $H \simeq 2/3$. Furthermore, very recently compatibility with $\mu \simeq 3/2$ was also reported in MD simulations [25].

In figure 8 we show the values of $\langle x_{\min}\rangle$, $P(\langle x_{\min}\rangle)$ and P_0 (estimated from the curves in figure 7) as a function of $N = L^2$. Dashed straight lines are displays of the exact power-laws $N^{-2/3}$ and $N^{-1/3}$, not fits. We can see that the prediction of equation (22) work remarkably well and equation (25) accompanies it perfectly. The original prediction for the scaling of
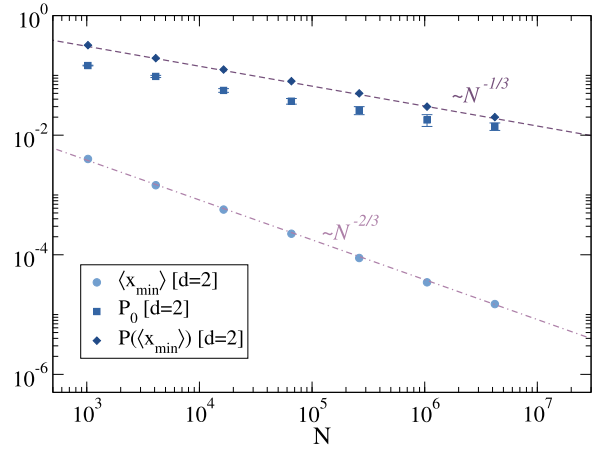
P_0 (equation (23)) is also good (as could be seen in the collapses of figures 7(b)–(c)), but we can also notice that P_0 is slowly merging with $P(\langle x_{\min}\rangle)$ as system size increases, and it is indeed when $N \to \infty$ when we expect them to be equal and equation (23) to hold.

4.2. Three-dimensional systems (3D)

Now, let us discuss the three-dimensional case. Contrary to the 2D case, where the few interaction kernels that one can choose (corresponding to the different kind of volume-preserving applied deformations) are symmetric under the exchange of q_x and q_y, in 3D the many different possibilities for choosing the elastic kernel all are non-symmetric respect to the permutations of q_x, q_y and q_z. The precise symmetry of the six independent deviatoric modes in 3D can be seen for example in [39]. The results we present here correspond exclusively to the kernel shown in equation (A7), where the way in which the z dimension enters differs from that of x and y. In figure 9 we show data similar to that in figure 7 but for the $d = 3$ case. We can first observe in the raw data of figure 7(a) that the determination of the θ exponent is more ambiguous than in $d = 2$. At intermediate values of x, say $\sim (0.005$–$0.1)$, a power-law region can be visualized and it has an exponent $\theta \simeq 0.35$–0.37, as reported in previous works [11, 14]. Yet, such a value for θ would imply $\mu = 2\theta \simeq 0.70$–$0.74 < 1$ and therefore $H > 1$. In that case, according to [21] the drift becomes dominant and we cannot expect the arguments related to the survival probability of x close to $x = 0$ to hold. Notice nevertheless that, for the largest system sizes, another power-law regime at smaller $x \sim (10^{-4}$–$10^{-3})$ is insinuated. We will come back on this when discussing systems with different aspect ratios, but let us advance that such power-law with a steeper slope would represent a more consistent value for θ in $d = 3$.

In any case, let us now discuss scalings for the data in figure 9. In figure 9(b) we see that the N dependence of $\langle x_{\min}\rangle$ an P_0 follows a power-law behavior like the one predicted by equations (22) and (23) but with clearly different exponents. Actually, the observed scaling is $\langle x_{\min}\rangle \sim N^{-7/9}$ and $P_0 \sim N^{-2/9}$. Using these values we rescale the $P(x)$ data to
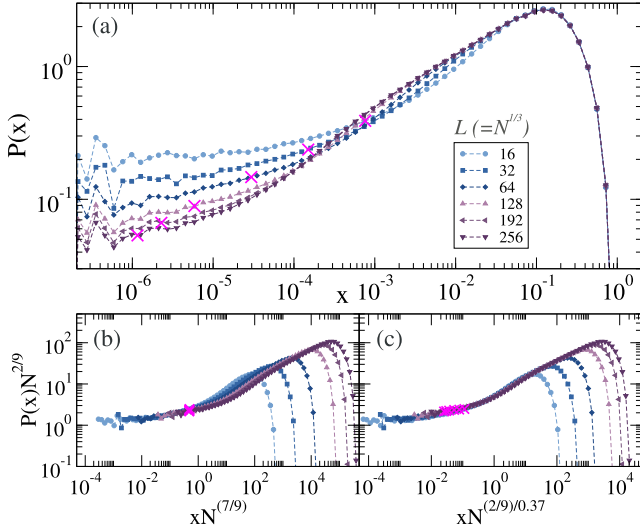
Figure 9. Distribution of local distances to threshold $P(x)$ in the quasistatic driven steady state of Picard's 3D model. (a) The $P(x)$ distributions. Different linear system sizes $L = \sqrt[3]{N}$ are represented with different colors/symbols as declared in the label. Pink crosses indicate the location of $\langle x_{\min} \rangle$ for the different system sizes. (b) $P(x)N^{2/9}$ vs $xN^{2/3}$ testing the scalings of equations (22) and (23). (c) $P(x)N^{2/9}$ vs $xN^{(2/9)/0.37}$ to preserve the power-law regime $\sim x^{\theta}$ with $\theta = 0.37$ observed in the main plot at intermediate values of x.

Figure 10. Dependence of $\langle x_{\min} \rangle$, P_0 and $P(\langle x_{\min} \rangle)$ with system size N for (cubic box) 3D Picard's model.

obtain figure 9(b). Again, notice that as in the case of $d = 2$ the collapse of the points $[\langle x_{\min} \rangle, P(\langle x_{\min} \rangle)]$ (equations (22) and (24)) is better than the scaling of the plateaus, which are even hard to define. If we further consider the power-law regime with an exponent $\theta \simeq 0.37$ we can do as in the $d = 2$ case and produce figure 9(c), for completeness.

In figure 10 we show the values of $\langle x_{\min} \rangle$, $P(\langle x_{\min} \rangle)$ and P_0 (estimated from figure 9) as a function of $N = L^3$ for $d = 3$. Dashed straight lines simply display the power laws $\sim N^{-2/9}$ and $\sim N^{-7/9}$, they are not fits. The measured values shown in figure 10 follow these trends very well. These values do not coincide with the predictions of equations (22) and (23). We believe the main reason is that our argumentation in the previous section implicitly assumed that all spatial dimensions of the system participate on the same footing. As we already stressed it, while the $d = 2$ Eshelby propagator (equation (A2)) is in fact symmetric against exchange of axis, this is not the case for the $d = 3$ propagator (equation (A7)).

We can provide a partial explanation for the values found for the N dependence of $\langle x_{\min} \rangle$ and $P(\langle x_{\min} \rangle)$ (or P_0) in 3D in the following way. First of all, notice that for $q_z = 0$ the three dimensional kernel (equation (A7)) reduces to the two dimensional one (equation (A2)). We will make the assumption that the non-trivial scaling of $\langle x_{\min} \rangle$ is still governed by the finite-kick walk analysis that we did in section 3, but in which the z coordinate has to be treated as a 'dumb' independent dimension. This is, let us think on the $d = 3$ case as a collection of several $d = 2$ systems stacked in the z direction, and evolving in parallel. If we take, L_z systems of size $L \times L$ and choose after each avalanche the minimum x among all of them, we would have a $\langle x_{\min} \rangle$ scaling as

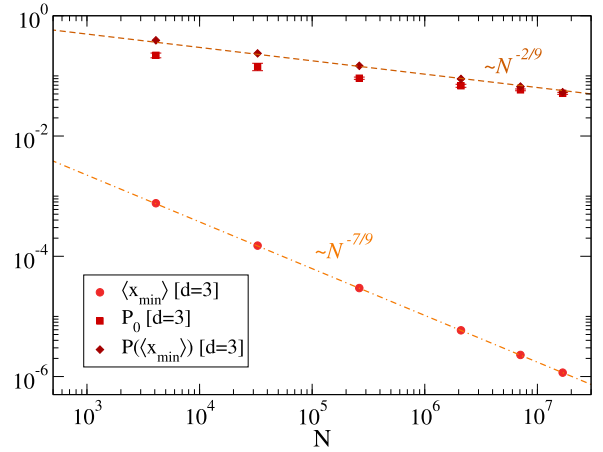$$\langle x_{\min} \rangle \sim L^{-4/3} L_z^{-1} \qquad (26)$$

and

$$P_0 \sim L^{-2/3} \qquad (27)$$

(note that P_0 turns out to be independent of L_z). When $L_z = L$ this leads to the scaling $\langle x_{\min} \rangle \sim N^{-7/9}$ and $P_0 \sim N^{-2/9}$ (with $N = L^3$) that we observe in figure 8. In fact, simulations in systems with different $L_x = L_y = L$ and L_z show that equations (26) and (27) are very well satisfied, as we will see in the following.

Figure 11 shows the scaling of $\langle x_{\min} \rangle$ for different cases. First, the $N = L^3$ case is reproduced from figure 10 for comparison. Then, we increase the system size while fixing $L_x = L_y$ and varying only L_z (the dimension perpendicular to the shear plane, that enters in a 'different' way than the other two in the propagator (A7)). This yields a scaling $\langle x_{\min} \rangle \sim N^{-1}$ controlled by $\langle x_{\min} \rangle \sim L_z^{-1}$ since the system size in the other two dimensions is fixed. Finally, we do inversely and we increase the system size by growing $L_x = L_y$ and keeping L_z fixed. This yields a scaling $\langle x_{\min} \rangle \sim N^{-2/3}$ controlled by a scaling of $\langle x_{\min} \rangle \sim L^{-4/3}$ (equation (26)) for both L_x and L_y. Notice that when the system size is increased in this way (at a fix perpendicular direction to the shear plane) we recover the scaling observed in the MD simulations of [7–9], that shows no exponent difference between $d = 2$ and $d = 3$.

In figure 12 we take a look to the $P(x)$ distributions in these asymmetric boxes for different aspect ratios. On one hand, we have fixed $L_x = L_y = 64$ and vary L_z between 8 and 384. On the other hand, we have fixed $L_z = 64$ and vary $L_x = L_y$ between 16 and 512. Notice first that, when L_z is the only changing dimension, the plateau level actually increases, with a small positive power, and it seems to saturate for large sizes around $P_0 \sim 0.12$. So, the strong $\langle x_{\min} \rangle$ scaling decreasing as $1/N$, is accompanied by a barely changing P_0 with N, as we could have expected from equation (20). These curves for $P(x)$ have the particularity that they only show a power-law regime at 'large' values of x, and they correspond to an 'abnormally small' value of θ, coincident with the many times reported [11, 14] but never truly justified $\theta \simeq 0.35$–0.37 in 3D. This θ value would point to $\mu < 1$, beyond the assumptions used for the derivation of our scaling arguments.
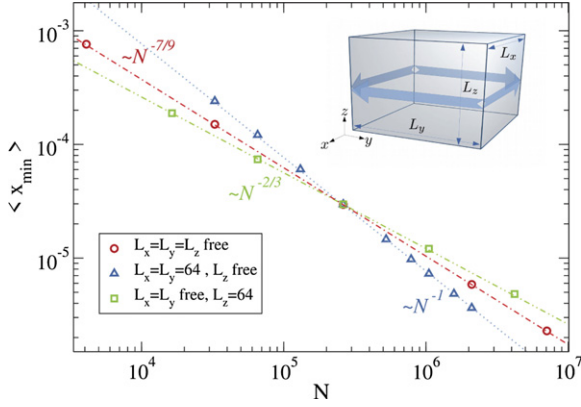
Figure 11. Dependence of $x_{\min}$ with system size N for the 3D Picard's model with different aspect ratios. The sketch of the inset represents the 3D simulation box with its dimensions L_x, L_y and L_z, and arrows indicating the strain deformation that gives rise to the propagator that we use for $d = 3$ in this work (equation (A7)).
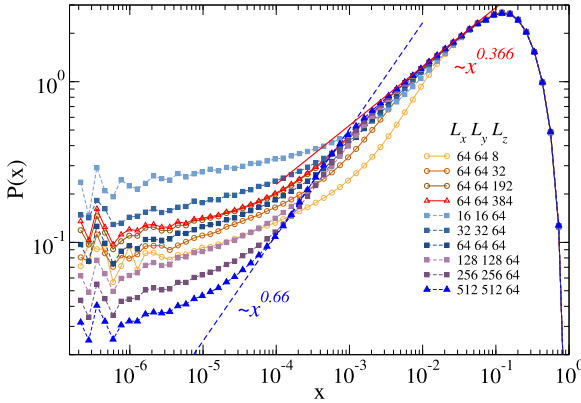

Figure 12. $P(x)$ for Picard's 3D model with different aspect ratios. For the largest system size of each size grow scheme (varying $L_x = L_y$ or varying L_z), the power-law regime visible at the smallest values of x is marked by a straight line to guide the eye.

Now, if we analyze the curves when varying $L_x = L_y$ at fix L_z things change dramatically. First, the plateau level is 'well behaved' decreasing as N increases. In fact, a reasonable $P_0 \sim N^{-0.3}$ accompanies the scaling of $x_{\min}$ shown in figure 11 for this case. Secondly, the larger system sizes clearly display a different power-law at intermediate x values, with $P(x) \sim x^{0.66}$ in such range. As it stands closer to the boundary $x = 0$, that will be the power-law dominating the system's dynamics close to the transition (e.g., the value of the flowcurve exponent β [15, 16]). In fact, in $d = 3$, $H = 1/(2\theta) \simeq 0.75$–$0.77$ is expected [16], consistent with $\theta \simeq 0.65$–0.66. Moreover, $\theta \simeq 0.66$ suggests a value of $\mu = 2\theta \simeq 1.33$ in $d = 3$, which brings the problem back into the range of validity of our general assumptions for the derivation of the scalings ((22) and (23)).

It needs to be stressed that the occurrence of these two clearly different finite size scalings in 3D—(i) growing the system in the direction perpendicular to the shear plane or (ii) growing the system in the directions of the shear plane—remains as an open issue (see discussion below).

5. Summary and discussion

In this paper we have considered the problem of the strain load $\Delta\gamma$ needed to trigger consecutive avalanches in the steady state of quasistatically deformed amorphous solids. In particular, we studied the finite-size scaling of its mean value $\langle\Delta\gamma\rangle$. The values of $\Delta\gamma$ are intimately related to the distribution $P(x)$ of local distances to instability x; $\langle\Delta\gamma\rangle$ is simply proportional to the average value of the minimum x across the system, namely $\langle\Delta\gamma\rangle \sim \langle x_{\min}\rangle$. We have built a theoretical argument starting by simple random walks of x with an absorbing boundary to show how the effect of a *discrete* step induces a finite value of $P(x)$ at the boundary. Then, we stood on an alternative mean-field modeling approach for the yielding phenomena [15, 17], considering as the physically relevant case the one in which the mechanical noise is generated by extended and collective plastic events, leading to a fat tail noise distribution $w(\xi) \sim |\xi|^{-(\mu+1)}$ with $1 < \mu < 2$. The mechanical noise generated by these avalanches has indeed a discrete nature, and therefore the distribution of $P(x)$ is expected to acquire a finite value as $x \to 0$, namely $P(x \to 0) = P_0 \neq 0$. More importantly, the discreetness in the mechanical kicks is not the trivial $\sim 1/N$ finite-system effect, but one that has to do also with the mean avalanche size in the system (e.g., see equation (18)). This holds for any $1 < \mu < 2$ and we explicitly derive the P_0 vs N scaling in that case. The scenario is confirmed by extensive numerical simulations of a classical elastoplastic model in 2 and 3 dimensions.

Even though the value of P_0 decreases to zero as $N \to \infty$, and therefore it could be naively considered a finite-size effect, its behavior with system size happens to be precisely what governs the scaling of $\langle x_{\min}\rangle$, and thus of $\langle\Delta\gamma\rangle$, our quantity of interest. Our theoretical analysis is able to justify a universal dependence $\langle\Delta\gamma\rangle \sim N^{-\alpha}$, with $\alpha = 2/3$, independent of spatial dimension and system parameters, as is actually found in MD simulations [7, 8]. Moreover, we have no need to assume a particular shape for the energy barriers [8] in doing so. It is worth mentioning nevertheless, that, as most of the numerical literature on the field, our construction assumes so far an athermal system. In this case the dynamics is dominated by the minimal value of distance to instability, $x_{\min}$, at every loading step. A finite temperature in a thermodynamic system ($N \to \infty$) may blur this (otherwise strictly) extremal dynamics. It might be an interesting problem for future works to analyze how our predictions are impacted by a finite temperature.

In the numerical results presented here for EP models in $d = 2$ the value $\alpha = 2/3$ is clearly obtained. However, the corresponding results in symmetric (i.e., cubic) $d = 3$ systems display a different value $\alpha \simeq 7/9$. We have identified a possible reason for this discrepancy in $d = 3$ in an unforeseen $\langle x_{\min}\rangle$ scaling dependence with the linear size of the sample along different directions relative to the externally applied shear. In contrast with the $d = 2$ case, the interaction kernel in $d = 3$ is not symmetric in all coordinates. Growing the system in the direction perpendicular to the shear plane has an effect markedly different on $\langle x_{\min}\rangle$, than growing it in the other directions. By studying $d = 3$ systems of different aspect ratio we addressed these multiple scalings, showing that in the case

in which the dimension perpendicular to the shear plane is kept fixed, $\alpha \simeq 2/3$ is recovered even in $d = 3$ EP systems. The different scalings of $\langle x_{\min} \rangle$ and P_0 with the different linear dimensions of a 3D system can be rationalized by a Gedanken problem in which the 3D system behaves as a collection of independent 2D systems. However, there is no basis to expect that this is actually the way in which a 3D system behaves and we know that the dynamics of interactions is more complex than that. The kernel asymmetry might be a weakness of the EP simplification and non-physically dominant at the end of the day. This is what one could interpret from the fact that classical MD results [7–9] maintain the $\langle x_{\min} \rangle \sim N^{-2/3}$ scaling. Moreover, a recent proposal of 'augmented' elastoplastic models tries to incorporate (among other things) the fact that shear strain in any direction due to a rearrangement can trigger the next rearrangement equally well. Successive rearrangements observed in MD are 'isotropically distributed' and not concentrated in the strain direction prescribed by the imposed deformation [40]. If the interaction kernel is symmetrized somehow our predictions equations (22) and (24), turn to be valid in the elastoplastic 3D case as well. We have checked this so far for synthetic, non-physical, kernels only (data not shown).

In any case, a definite value of α implies additional predictions on other critical exponents of the yielding transition. For instance, the avalanche distribution exponent τ and the fractal dimension of avalanches $d_{\rm f}$ are linked to α through [11, 15]

$$d\alpha = d - d_{\rm f}(2 - \tau), \tag{28}$$

(note that this relation is usually written using θ instead of α, by applying the extra assumption $\alpha = 1/(1 + \theta)$, that we consider not justified in the steady state). A unique value $\alpha = 2/3$ in $d = 2$ implies $d_{\rm f}(2 - \tau) = 2/3$. Most of the values reported in the literature satisfy this relation. In particular, we have tested for six different EP models [15] $d_{\rm f} \simeq 1$ and $\tau \simeq 1.33$. For $d = 3$, we must still understand which is the value of α that we should expect, but $d_{\rm f}$ and τ could also suffer from an asymmetry effect if equation (28) is expected to hold.

Finally, all this picture should be compatible with known results for the as-quenched state; with rigorous power-laws for $P(x_{\min})$ and $P(x)$ at small arguments. We believe that the effective mechanical noise governing the distribution $P(x)$ and its properties, like the one that defines the finite-size scaling of $\langle x_{\min} \rangle$, must display systematic biases in the non-universal transient. While we will not venture to link transient values of μ (or H) with θ in such a regime (which, furthermore, is only measurable on a given system size for certain ranges of initial annealing), our guess is that avalanches progressively build up and their geometry—encoded in $d_{\rm f}$ [11, 20]—varies with strain, therefore modifying the effective noise, until it reaches a steady distribution governed by $1 < \mu < 2$.

6. Conclusion

In conclusion, we have provided a novel interpretation of the finite size scaling of $\langle \Delta \gamma \rangle$ in the steady state of amorphous systems under deformation. This interpretation seems to conciliate MD simulation results and EP constructions, otherwise in

contradiction in this limit. While the hypothesis of a marginal stability behavior, rooted in the celebrated $P(x) \sim x^{\theta}$ pseudo-gap, has been proved to hold in the as-quenched isotropic state of model glasses [7, 8] and still renders important outcomes in the transient [20, 24], it does not seem to apply 'as-is' to the steady state case. There, at least, the system dynamics is correlated at the level of avalanches and this naturally produces a finite value of $P(x)$ as $x \to 0$, when observing the $P(x)$ distribution in the quasistatic limit, justified on a discrete step for the effective dynamics of the x values. This behavior of $P(x)$ does not invalidate the essence of the yielding transition, anchored in the sub-extensive scaling of $\langle \Delta \gamma \rangle^{-1}$; since the level of such asymptotic plateau at small x is itself dependent on N and is shown to govern the behavior of $\langle \Delta \gamma \rangle \sim N^{-\alpha}$, independently on θ.

Some questions remain open, and we hope they will motivate further endeavors on the subject. But we believe that this is a first step in shedding light on a probable misconstruction in the field, based in a wrong extrapolation of arguments valid in the early deformation regime to the steady state case.

Data availability statement

All data that support the findings of this study are included within the article (and any supplementary files).

Appendix A. Elastoplastic model and simulation protocol

EP models are intended to describe amorphous materials at a coarse-grained-level, laying in between the particle-based simulations and the continuum-level description [5]. In short, the amorphous solid is represented by a coarse-grained scalar stress field $\Sigma(\boldsymbol{r}, t)$, at spatial position $\boldsymbol{r}$ and time t under an externally applied shear strain. Space is discretized in blocks (e.g., square lattice). At a given time, each block can be 'inactive' or 'active' (i.e., yielding). This state is defined by the value of an additional variable: $n(\boldsymbol{r}, t) = 0$ (inactive), or $n(\boldsymbol{r}, t) = 1$ (active). An over-damped dynamics is imposed for the stress on each block, following some basic rules: (i) the stress loads locally in an elastic manner while the block is inactive. (ii) When the local stress overcomes a local yield stress, a *plastic event* occurs with a given probability, and the block becomes 'active' ($n(\boldsymbol{r})$ is set to one). Upon activation, dissipation occurs locally, and this is expressed as a progressive drop of the local stress, together with a redistribution of the stresses in the rest of the system in the form of a long-range elastic

perturbation. A block ceases to be active when a prescribed criterion is met. The auxiliary binary field $n(\mathbf{r}, t)$ shows up in the equation of motion for the local stress $\Sigma(\mathbf{r}, t)$, defining a dynamics that is typically non-Markovian. While the structure of the equation of motion for the local stresses is almost unique in the literature, both its parameters and the rules governing the transitions of $n(\mathbf{r})$ ($0 \rightleftharpoons 1$) show a variety of choices.

We define our EP model as a d-dimensional scalar field $\Sigma(\mathbf{r}, t)$, with tipically $d = 2$ or 3, and $\mathbf{r}$ discretized on a square/cubic lattice and each block Σ_i subject to the following evolution in real space

$$\frac{\partial \Sigma_i(t)}{\partial t} = \mu \dot{\gamma}^{\text{ext}} + \sum_j G_{ij} n_j(t) \frac{\Sigma_j(t)}{\tau}; \qquad \text{(A1)}$$

where $\dot{\gamma}^{\text{ext}}$ is the externally applied strain rate, and the kernel G_{ij} is the Eshelby stress propagator [41].

It is sometimes convenient to explicitly separate the $i = j$ term in the previous sum, as

$$\frac{\partial \Sigma_i(t)}{\partial t} = \mu \dot{\gamma}^{\text{ext}} - g_0 n_i(t) \frac{\Sigma_i(t)}{\tau} + \sum_{j \neq i} G_{ij} n_j(t) \frac{\Sigma_j(t)}{\tau}; \quad \text{(A2)}$$

where $g_0 \equiv -G_{ii} > 0$ (no sum) sets the local stress dissipation rate for an active site. The form of G is $G(\mathbf{r}, \mathbf{r}') \equiv G(r, \varphi) \sim \frac{1}{\pi r^2} \cos(4\varphi)$ in polar coordinates, where $\varphi \equiv \arccos((\mathbf{r} - \mathbf{r}') \cdot \mathbf{r}_{\dot{\gamma}(\text{ext})})$ and $r \equiv |\mathbf{r} - \mathbf{r}'|$. For our simulations we obtain G_{ij} from the values of the propagator in Fourier space $G_{\mathbf{q}}$, defined as

$$G_{\mathbf{q}} = -\frac{4q_x^2 q_y^2}{(q_x^2 + q_y^2)^2}. \qquad \text{(A3)}$$

for $\mathbf{q} \neq \mathbf{0}$ and

$$G_{\mathbf{q}=\mathbf{0}} = -\kappa \qquad \text{(A4)}$$

with κ a numerical constant (see below). Note that in our square numerical mesh of size $L \times L$, q_x^2, q_y^2 must be understood as

$$q_{x,y}^2 \equiv 2 - 2\cos\left(\frac{\pi m_{x,y}}{L}\right) \qquad \text{(A5)}$$

with $m_{x,y} = 0, \ldots, L - 1$.

The elastic (e.g. shear) modulus $\mu = 1$ defines the stress unit, and the mechanical relaxation time $\tau = 1$, the time unit of the problem. The last term of (A2) constitutes a *mechanical noise* acting on Σ_i due to the instantaneous integrated plastic activity over all other blocks ($j \neq i$) in the system.

The picture is completed by a dynamical law for the local state variable $n_i = \{0, 1\}$. We define hereafter the rule corresponding to the Picard's model [37] that we use:

$$n_i : \begin{cases} 0 \to 1 & \text{at rate } \tau_{\text{on}}^{-1} \text{ if } \Sigma_i > \Sigma_{\text{th}i} \\ 0 \leftarrow 1 & \text{at rate } \tau_{\text{off}}^{-1}, \end{cases} \qquad \text{(A6)}$$

where τ_{on} and τ_{off} are parameters and $P(\Sigma_{\text{th}i}) = \delta(\Sigma_{\text{th}i} - 1)$. In $d = 3$, the Eshelby kernel for one scalar component of the deviatoric strain in Fourier space can be written as

$$G_{\mathbf{q}}^{\text{3D}} = -\frac{4q_x^2 q_y^2 + q_z^2(q_x^2 + q_y^2 + q_z^2)}{(q_x^2 + q_y^2 + q_z^2)^2} \qquad \text{(A7)}$$

and the dimensional extension of the dynamics is straightforward.

A.1. Quasistatic protocol

For the analysis of avalanche statistics, it is convenient to have a protocol that allows for the triggering and unperturbed evolution (no driving) of avalanches until they stop, guaranteed by a degree of stress non-conservation $\kappa > 0$ (we use $\kappa = 1$, as in previous strain-controlled EP models implementations [14, 42, 43], unless otherwise specified). This is the quasi-static protocol described here.

Starting from any stable configuration, i.e., no site is active and no site stress is above its local threshold ($n_i = 0$ and $\Sigma_i < \Sigma_{\text{th}i}$ for all sites), the next avalanche of plastic activity is triggered by globally increasing the stress by the minimum amount necessary for a site to reach its local threshold. That site (the weakest) is activated at threshold with no stochastic delays; it perturbs the stress values of other sites and the rest of the avalanche evolves without any external drive following the dynamics prescribed by equation (A2) (and the corresponding activation rule) with $\dot{\gamma} = 0$. The avalanche stops once there are no more active sites and all stresses are below their corresponding thresholds again. At this point the loading process is repeated. For each simulation run, data is collected only in the steady-state.

Appendix B. Model with a quenched random kernel

In this section we analyze the properties of a model with a different form of the interaction kernel. Instead of using the appropriate interaction to describe the properties of yielding, namely the Eshelby kernel presented in equation (A3), we consider a model in which the $G_{\mathbf{q}}$ kernel takes random values. In concrete, we use

$$G_{\mathbf{q}} = -\text{RND}(\mathbf{q}), \qquad \text{(B1)}$$

where RND($\mathbf{q}$) stands for an independent random number chosen from a flat distribution between 0 and 1 for each value of $\mathbf{q}$. Note that this is a 'quenched' random kernel, since the form of $G_{\mathbf{q}}$ is chosen once and for all at the beginning of the simulation [46].

Although this is probably not a realistic model to describe any physical situation, there are a few reasons that make the study of this model interesting. The first one concerns its relation with another version of a 'random' yielding model, namely the Hébraud–Lequeux (HL) model [44, 45]. In its essence, the HL model for a system with N sites considers that every time a single site performs a plastic re-accommodation, it produces a random kick of finite variance σ (with $\sigma \sim N^{-1/2}$) on every other site. Note however that in this case the values of the random kicks are refreshed at every plastic event [38]. From its very definition the mechanical noise in the HL model is a standard random walk, corresponding to a value of $\mu = 2$. In the quenched random case we are examining, we must first understand what are the properties of the uncorrelated mechanical noise felt by a particular target site. The quenched random

kernel $G_{\mathbf{q}}$ generates values G_r that are mostly uncorrelated spatially, and distributed with a finite variance σ. This is enough to guarantee that we will find a value $\mu = 2$ (and therefore [21] $\theta = 1$) as in the HL model. In addition, the dependence of σ on the number of sites N in the system is $\sigma \sim 1/\sqrt{N}$, as in the HL model. Then we can write down the scaling of P_0 with N from (the limit of validity of) equation (12), which is independent of the details of the kernel, as

$$P_0 \sim N^{-1/2} \tag{B2}$$

and also

$$\langle x_{\min} \rangle \sim N^{-1/2} \tag{B3}$$

thus finding in the present case a different scaling that the one given by equations (22) and (23). The arguments that led to equations (22) and (23) fail here because the scaling of σ with N obtained in equation (19) was based in the conservation of the number of large kicks when system size is increased (see figure 6), something that does not occur here because of the assumed non-decaying nature of the interactions.

We performed simulations with a quenched random kernel and evaluated the distribution $P(x)$, and the value of $\langle x_{\min} \rangle$. The simulations shown here were done in two spatial dimensions, but we verified that exactly the same results are obtained in three dimensions if the number of sites in the system is maintained. This is of course related to the fact that in a randomly interacting model dimensionality plays no relevant role.

Figure 13 shows the results of simulations with the random kernel. The upper panel shows the form of $P(x)$ for different values of N and we can see that the value $\theta = 1$ for $P(x) \sim x^{\theta}$ in an intermediate range of x is well established as N increases.

The lower panel shows the scaling of P_0 and $\langle x_{\min} \rangle$ with N, where we observe clearly the expected $\sim N^{-1/2}$ dependence.

ORCID iDs

Ezequiel E Ferrero ⓘ https://orcid.org/0000-0001-8516-6146
Eduardo A Jagla ⓘ https://orcid.org/0000-0003-4773-2308

References

[1] Carlson J M, Langer J S and Shaw B E 1994 *Rev. Mod. Phys.* **66** 657
[2] Fisher D S 1998 *Phys. Rep.* **301** 113
[3] Ferré J, Metaxas P J, Mougin A, Jamet J-P, Gorchon J and Jeudy V 2013 *C. R. Phys.* **14** 651 disordered systems/systèmes désordonnés
[4] de Gennes P G 1985 *Rev. Mod. Phys.* **57** 827
[5] Nicolas A, Ferrero E E, Martens K and Barrat J-L 2018 *Rev. Mod. Phys.* **90** 045006
[6] Maloney C and Lemaître A 2004 *Phys. Rev. Lett.* **93** 016001
[7] Lerner E and Procaccia I 2009 *Phys. Rev.* E **79** 066109
[8] Karmakar S, Lerner E and Procaccia I 2010 *Phys. Rev.* E **82** 055103
[9] Karmakar S, Lerner E, Procaccia I and Zylberg J 2010 *Phys. Rev.* E **82** 031301
[10] Lin J, Saade A, Lerner E, Rosso A and Wyart M 2014 *Europhys. Lett.* **105** 26003
[11] Lin J, Lerner E, Rosso A and Wyart M 2014 *Proc. Natl Acad. Sci. USA* **111** 14382
[12] Budrikis Z, Castellanos D F, Sandfeld S, Zaiser M and Zapperi S 2017 *Nat. Commun.* **8** 15928
[13] Tyukodi B, Patinet S, Roux S and Vandembroucq D 2016 *Phys. Rev.* E **93** 063005
[14] Liu C, Ferrero E E, Puosi F, Barrat J-L and Martens K 2016 *Phys. Rev. Lett.* **116** 065501
[15] Ferrero E E and Jagla E A 2019 *Soft Matter* **15** 9041
[16] Ferrero E E and Jagla E A 2019 *Phys. Rev. Lett.* **123** 218002
[17] Fernández Aguirre I and Jagla E A 2018 *Phys. Rev.* E **98** 013002
[18] Jagla E A 2018 *J. Stat. Mech.* 013401
[19] Salerno K M and Robbins M O 2013 *Phys. Rev.* E **88** 062206
[20] Lin J, Gueudré T, Rosso A and Wyart M 2015 *Phys. Rev. Lett.* **115** 168001
[21] Lin J and Wyart M 2016 *Phys. Rev.* X **6** 011005
[22] Hentschel H G E, Jaiswal P K, Procaccia I and Sastry S 2015 *Phys. Rev.* E **92** 062302
[23] Ji W, Popović M, de Geus T W J, Lerner E and Wyart M 2019 *Phys. Rev.* E **99** 023003
[24] Shang B, Guan P and Barrat J-L 2020 *Proc. Natl Acad. Sci. USA* **117** 86
[25] Ruscher C and Rottler J 2020 *Soft Matter* **16** 8940
[26] Lin J and Wyart M 2018 *Phys. Rev.* E **97** 012603
[27] As a matter of fact, different values for the exponent θ are presented in reference [11] when either fitted from the $P(x)$ distribution or computed from the 'extremal dynamics' (the scaling of $x_{\min}$) through equation (7); 'a difference presumably resulting from corrections to scaling' according to the authors.
[28] Tyukodi B, Vandembroucq D and Maloney C E 2019 *Phys. Rev.* E **100** 043003
[29] Karimi K, Ferrero E E and Barrat J-L 2017 *Phys. Rev.* E **95** 013003
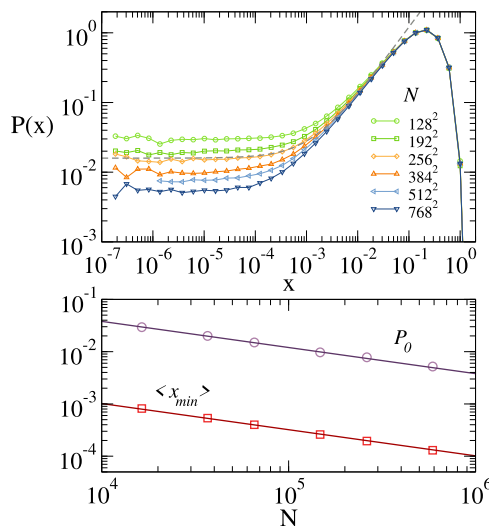[30] Lemaître A and Caroli C 2007 arXiv:0705.3122

Figure 13. (a) The form of $P(x)$ for system with different number of sites N in the quenched random kernel case. The dashed line displays the expected behavior $P(x) = C_1 + C_2 x$ on the $N = 256^2$ data. (b) The scaling of P_0 and $\langle x_{\min} \rangle$ with N. Symbols are the result of simulations. Straight lines indicate the expected $\sim N^{-1/2}$ dependence.

[31] Parley J, Fielding S and Sollich P 2020 *Phys Fluid* **32** 127104

[32] In the simulations presented here the reinjection is made randomly and uniformly in the full interval (0, 1).

[33] We thank D Vandembroucq for pointing this out.

[34] Note that instead of using at each step the latest $x_{\min}$ to define the distribution $w(\xi)$, one could use the self-tuned mean value $\mathrm{x}_{\min}$ and the conclusions are identical.

[35] In fact the largest kicks are produced by neighbor avalanches, the coarse-grained lattice description imposes the upper cut-off of the kick distribution, the minimal distance.

[36] See appendix B for the discussion of a case in which the assumptions made to derive this result do not apply, and then equation (19) does not hold.

[37] Picard G, Ajdari A, Lequeux F and Bocquet L 2005 *Phys. Rev.* E **71** 010501

[38] $x_{\min}$ is independently computed for each system size as the arithmetic average of the minimum x values (in the $L \times L$ system) for each after-avalanche configuration in the steady state.

[39] Jagla E A 2020 *Phys. Rev.* E **101** 043004

[40] Zhang G, Ridout S and Liu A J 2020 arXiv:2009.11414

[41] Picard G, Ajdari A, Lequeux F and Bocquet L 2004 *Eur. Phys. J.* E **15** 371

[42] Martens K, Bocquet L and Barrat J-L 2012 *Soft Matter* **8** 4197

[43] Nicolas A, Martens K and Barrat J-L 2014 *Europhys. Lett.* **107** 44003

[44] Hébraud P and Lequeux F 1998 *Phys. Rev. Lett.* **81** 2934

[45] Agoritsas E, Bertin E, Martens K and Barrat J-L 2015 *Eur. Phys. J.* E **38** 71

[46] It has to be emphasized that when using a quenched kernel as in this case, there is a stability condition expressed in the fact that $G_{\mathbf{q}}$ has to be non-positive, otherwise we would obtain exponentially growing modes. This is why we define the random kernel in $\mathbf{q}$ space. If we define a random kernel in real space instead, the negativity of $G_{\mathbf{q}}$ cannot be easily fulfilled.